JTTEE5 4:342-346


# Study of $Cr_2O_3$ Coatings Part I: Microstructures and Modulus

*C.S. Richard, J. Lu, G. Béranger, and F. Decomps*

**Metallographic characterization has been used to estimate the quality and, particularly, the adhesion of plasma-sprayed $Cr_2O_2$ coating. This study focuses on the state of the substrate before spraying. During the process of spraying, the differential contraction generated between the various materials because of their different physical and mechanical properties determines the stresses inside the coating and at the interface between the coating and the substrate. The residual stresses thus influence the mechanical and thermomechanical behavior of the coated parts and their adhesion. These stresses are determined by a step-by-step hole drilling method (Part II of this paper), and Young's modulus is measured by two different methods: a dynamic ultrasonic test and a static four-point bend test. Part II of this paper is devoted to the adhesion of a $Cr_2O_3$ deposit on a cast iron substrate.**

## 1. Introduction

THE USE of plasma-sprayed coatings has proliferated in a variety of aerospace and automobile applications. This widespread use is attributed to the fact that, quite often, materials in monolithic form are not suitable for the diverse and special requirements, and coatings provide appropriate technological solutions.

Plasma-sprayed ceramic coatings in combustion chambers of alternative car engines have been successfully developed for the thermal protection of components such as pistons, valves, upper liners, etc. Recently, Renault Automobiles Company developed plasma-sprayed chromium oxide coatings for application to components such as piston rings. These coatings are used to provide resistance to abrasion and wear at high temperature and to reduce friction (piston rings work in dry sliding conditions at 350 °C) (Ref 1).

Wear is closely related to the adhesion of the coating to the substrate because if the adhesion is poor, the coating will wear off quite rapidly and the extent of deterioration of the substrates by environmental factors will be greatly accelerated.

Adhesion is very important for determination of the life of coated parts. The coatings must be properly bonded to the substrates. Adhesion depends on surface preparation. Very few papers have specifically dealt with this problem or the effects of preparation (sandblasting, induced roughness) on adhesion.

Therefore, the following areas were selected for investigation: inspection of the substrate for factors such as roughness, residual stresses generated by sandblasting, and contamination by corundum which may affect bond strength. The second part is devoted to the evaluation of coating quality including metallographic characterization. The third section concerns determination of Young's modulus.

**Keywords** APS coating, ceramic, chromium oxide, four-point bend test, ultrasonic method, Young's modulus

**C.S. Richard** and **G. Béranger,** UTC, LG2mS, URA No. 1505, Département Génie Mécanique, 60200 Compiégne Cedex, France; **J. Lu,** CETIM, 60304 Senlis Cedex, France; and **F. Decomps,** Renault Automobiles, 92109 Boulogne-Billancourt, France.

## 2. Experimental Procedure

### 2.1 *Plasma Spraying*

The specimens in this investigation were produced by atmospheric plasma spraying (APS-Plasma Technik System, Plasma Technik, Wohlen, Switzerland) on graphite cast iron substrates that have been sandblasted with three types of corundum. The three grit blast media are referred to as 1, 2, and 3 and give rise to correspondingly coarse, medium, and low surface roughnesses (Table 1). A commercial chromium oxide powder was used as the feedstock (particle size distribution: 5 to 25 μm). The geometry of samples was 30 mm by 40 mm by 10 mm. The coating thickness was 500 ± 50 μm. The spraying parameters were the same for each type of specimen and are considered as proprietary information to Renault.

### 2.2 *Roughness*

Roughnesses for the three types of surfaces before plasma spraying were measured by a Taylor Hobson-6 Talysurf apparatus (Rank Taylor Hobson Limited, Leicester, England). Three dimensional roughness profiles were determined by an optical sensor (argon laser) with a charge-coupled device (CCD) video camera, acquisition and enhancement software, and roughness determination software.

### 2.3 *Residual Stress Profiles*

Residual stress distributions on each sample were determined by a modified step-by-step hole drilling method (incorporating the special software of CETIM-METRO) developed at CETIM.

**Table 1 Characteristic Roughnesses Obtained**

| | Roughness, μm | | |
|---|---|---|---|
| Specimen | $R_{max}$ | $R_{tm}$ | $R_{pm}$ |
| C1A | 55 | 40 | 18 |
| C2A | 50 | 37 | 17 |
| C3A | 27 | 22 | 11 |

Note: $R_{max}$ is the maximum peak-to-valley height. $R_{tm}$ is the mean depth of roughness. $R_{pm}$ is the mean depth of surface smoothness.

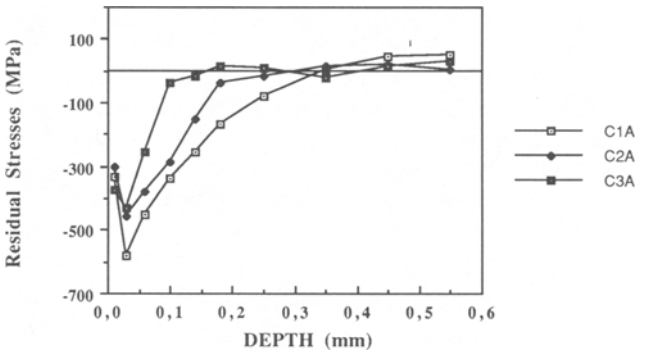


**Fig. 1** Comparison of residual stresses of C1A, C2A, and C3A substrates measured by the hole drilling method

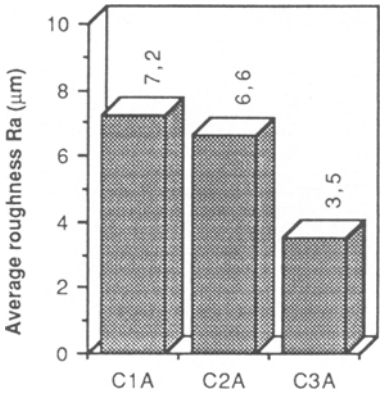


**Fig. 2** Average roughness, $R_a$. Each column represents the mean value for 8 measurements.

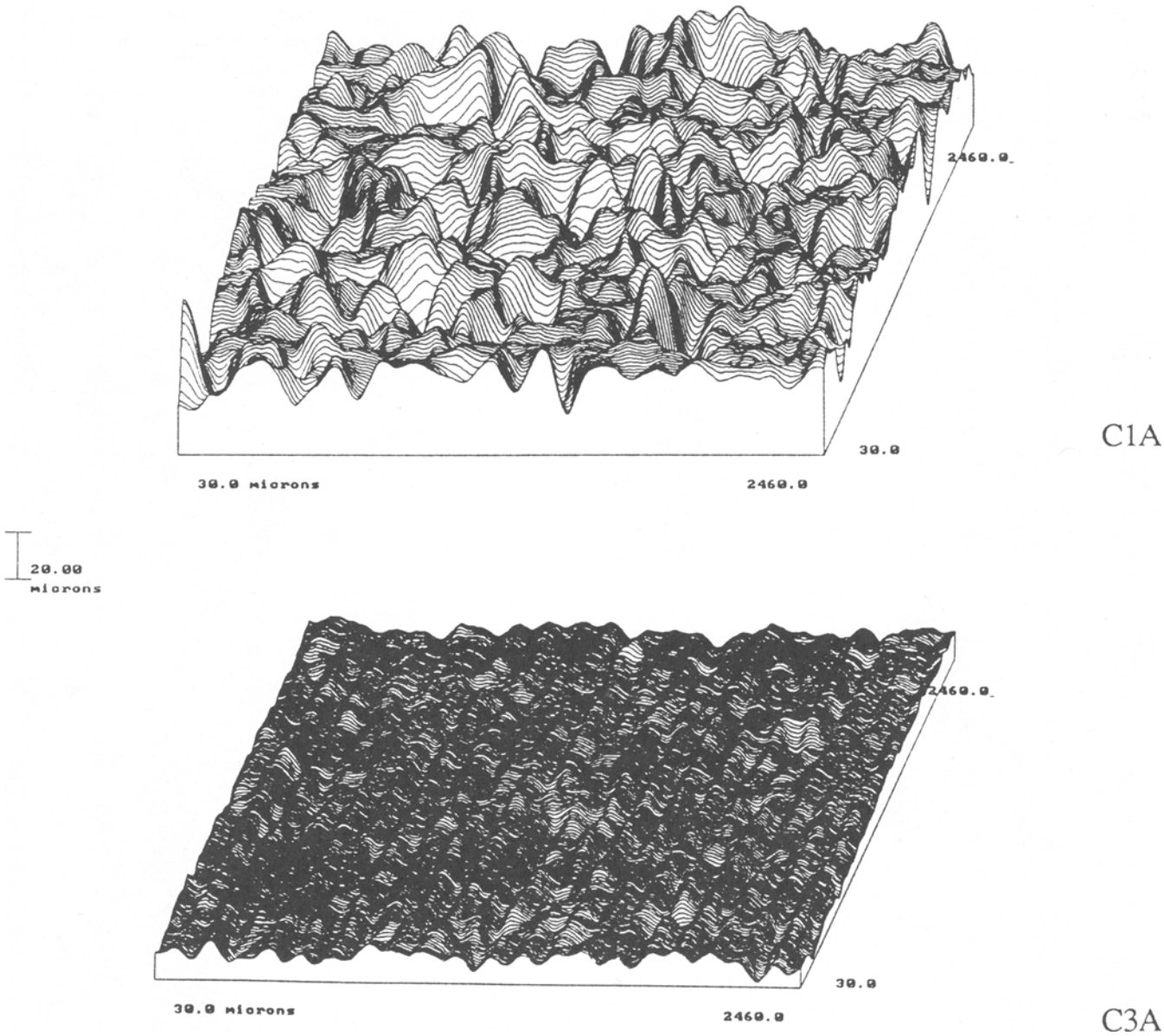


**Fig. 3** Three-dimensional representation of the results of roughness for C1A and C3A. Each edge of the test area ranges from 30 to 2460 µm. The vertical scale of 20 µm is not proportional to the *x*-*y* scales.

### 2.4 *Young's Modulus (E) Evaluation*

The ultrasonic measurements were carried out with a 5 MHz nonfocused transducer in full water immersion made with a bandwidth from 0.15 to 75 Hz, a maximum gain of 60 dB, and no damping. For the four-point bend test, longitudinal microstrain gages from Vishay Measurements Group, Inc. (Raleigh, USA) were used. The displacement sensor and the test apparatus were manufactured at CETIM.

## 3. Results

### 3.1 *Roughness of the Substrates*

The aim of sandblasting is often to induce compressive stresses on the surface (Fig. 1) to ensure the mechanical bonding of particles to the substrate and to clean the surface. Three types of specimens were used in this study; they are noted as C1A, C2A, and C3A. The number designates the level of roughness: 1 is for a coarse roughness, 2 is for a medium roughness, and 3 is for a low roughness. The different roughnesses were obtained by three types of corundum shot particles with the same blasting conditions.

The average roughness, $R_a$, results for the three samples studied are shown in Fig. 2. Table 1 exhibits the other characteristic values of roughness. Figure 3 presents two rough surfaces before plasma spraying in three-dimensional representation. The C1A and C2A substrates were similar, whereas the C3A substrate was completely different.

### 3.2 *Characterization of Coating Quality*

#### 3.2.1 Surface State

Observation of the coating microstructure underlines the lamellar packing, which is associated with the manufacture process (Fig. 4). Microcracking of each lamella arises from the thermal contractions generated by cooling (Fig. 5). The other surface features are composed of unmelted particles and deep pores between splashed particles. The trace of melted particles is not accurately revealed, but the first layer is soon to be the replica of the sandblasted surface of the substrate on which the first melted particles have splashed (Fig. 6).

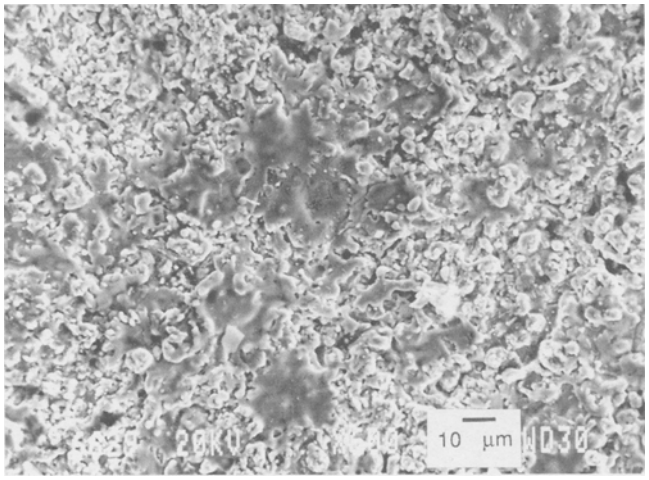


**Fig. 4** Surface of APS chromium oxide coating. Sample C1A

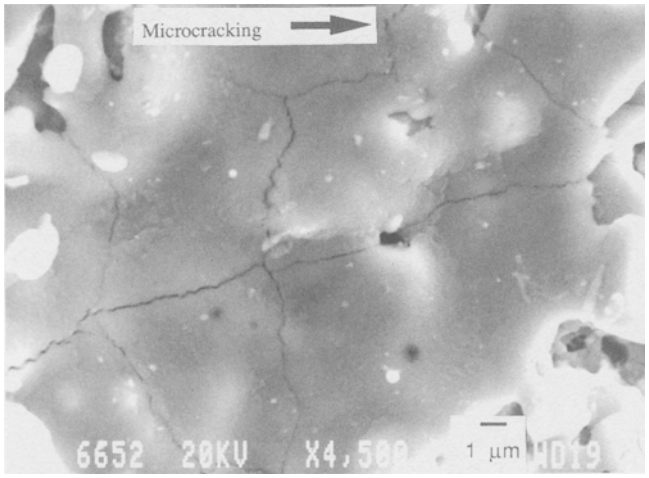


**Fig. 5** Microcracking of a lamella. Sample C1A

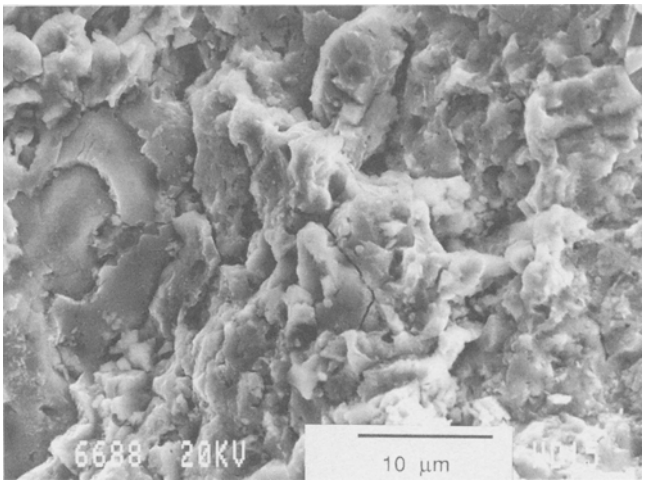


**Fig. 6** Interface of chromium oxide coating. Sample C1A

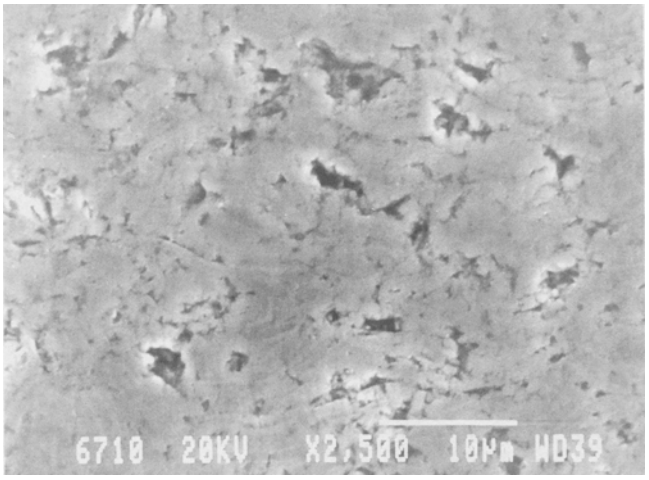

**Fig. 7** Cross section of C2A specimen

### 3.2.2 Structure in Depth

The structure in depth is still lamellar. Polished cross sections reveal wavy layers where the outline of each lamella can be distinguished (Fig. 7). Microcracking in the coating is also observed. The macroscopic texture, consisting of a classical lamellar structure and microcracking, is very important in explaining the mechanical behavior of coatings.

### 3.2.3 Crystallographic Structure

The analysis in cross section shows that the chromium oxide coating is relatively pure. The presence of some chromium-rich particles is observed. They may arise from the powder and/or are formed during the spraying by reduction of $Cr_2O_3$. (This phenomenon is more probable under the vacuum plasma spray processing.)

Tronche et al. (Ref 2) noted that atmospheric plasma spraying (APS) chromium oxide coatings have an identical composition with the powder. The authors also observed some white areas. They may correspond to $CrO_2$ suboxide. However, this phase is virtually undetectable by x-ray (Fig. 8). The presence of this second phase in the coating is confirmed by electron dispersive x-ray analysis (EDAX) and scanning electron microscopy (SEM) imaging.

### 3.2.4 Diffusion Measurements

Concentration distributions of iron and chromium were made in the boundary layer $Cr_2O_3$ deposit. An electron probe x-ray microanalyzer was used for the measurements. On a cross section of the coated plate, a line scan parallel to the interface was made to determine the concentration distributions of the elements in the substrate and in the coated layer. An example of the concentration curves is given in Fig. 9. No diffusion of Cr into the substrate or of Fe into the coating is observed in this case.

## 3.3 *Young's Modulus (E) Evaluation*

The stress-strain behavior, stress field at the interface, surface hardness, coating delamination, cracking, spalling, bending and residual stress of coated systems (Ref 3) all depend on the elastic modulus, $E$, of the coating. As a result, the elastic modulus of the coating is a fundamental parameter for characterizing coating performance. $E$ must be determined to measure residual stress distributions (more details are presented in Part II of this paper). Two methods were used. The first is a dynamic measurement, and the second is a static measurement from mechanical testing.

### 3.3.1 Dynamic Resonance Method

The ultrasonic pulse echo technique was used (Ref 4), with water as the ultrasound coupling medium (Fig. 10). The first specimen was examined from the substrate side (Fig. 10a). The second one was examined from the coating side (Fig. 10b).

The time difference between echoes $e_2$ and $e_3$ (or $e'_1$ and $e'_2$) was determined. The mean $\Delta t$ was 159 ± 10 ns. This result allowed the velocity of longitudinal waves, $V_L$, in the chromium oxide coating to be calculated as 6289 ± 1024 m/s.

The large estimated measurement error in this result can be due to roughness and porosity. The velocity of transverse waves, $V_T$, was determined under the same experimental conditions by evaluation of the Rayleigh angle; $V_T = 4350$ m/s.

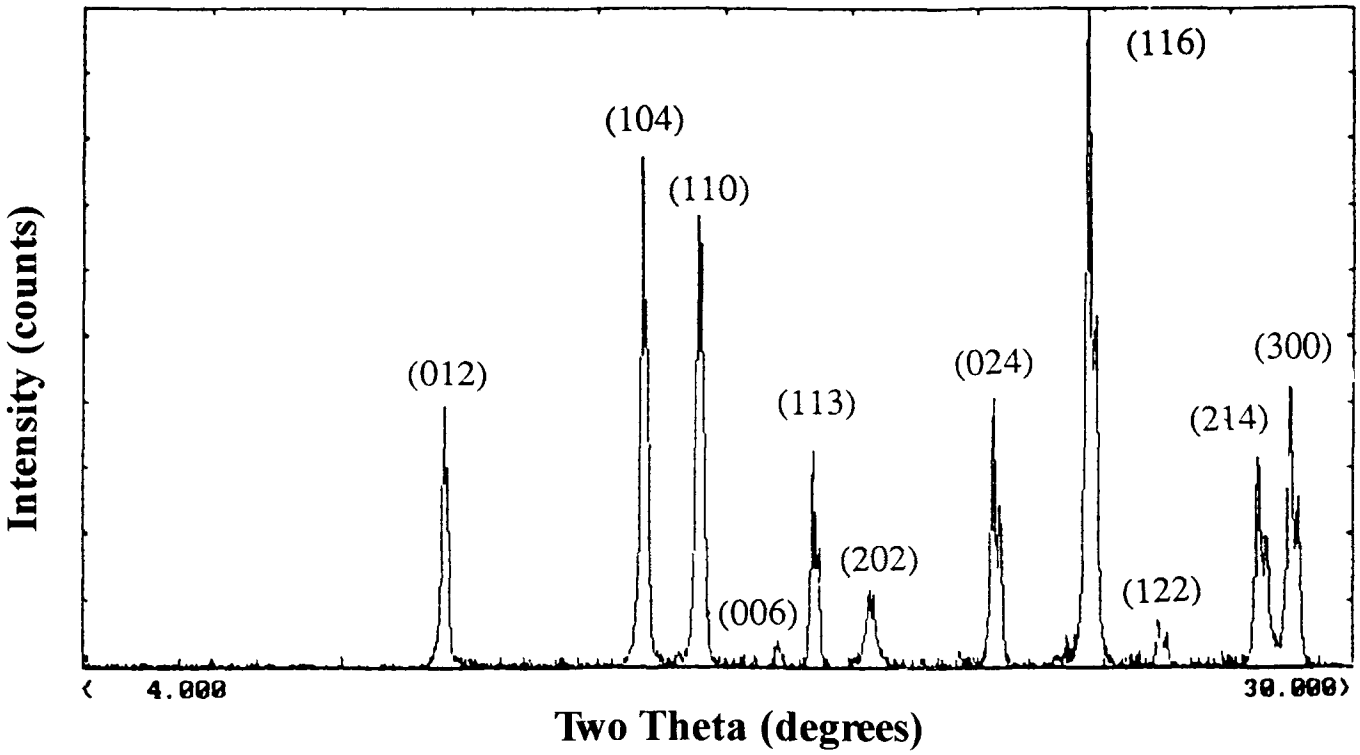


**Fig. 8** X-ray diffraction pattern of APS chromia coating

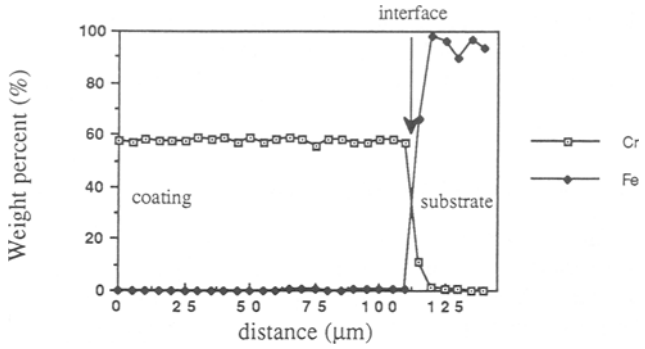


**Fig. 9** Concentration distributions of iron and chromium for $Cr_2O_3$ coating on a cast-iron substrate

The error was not evaluated because only one sample was tested. The Young's modulus is deduced from the equation:

$$E_{exp} = \rho_{exp} V_T^2 \frac{3(V_L)^2 - 4(V_T)^2}{(V_L)^2 - (V_T)^2} \quad \text{(Eq 1)}$$

where $E_{exp}$ is the experimental elastic modulus and $\rho_{exp}$ is the experimental density. In our case, $\rho_{exp}$ is 3500 kg/m$^3$. (The theoretical density is 5220 kg/m$^3$ for the bulk material, Ref 5.)

The $E_{exp}$ of APS chromium oxide is 138 GPa. This value is low in comparison to the 314 GPa (Ref 5) for fully dense chromium oxide. A static bend test was also carried out to check the dynamic value determined above.

### 3.3.2 Static Mechanical Method

The second method performed was a four-point bending test. $E_{exp}$ can be evaluated from the surface strains, $E_c$ and $E_s$ (respectively in the coating and in the substrate), which can be detected using strain gages attached to the specimen loaded in four-point bend (Fig. 11). The Young's modulus is determined by the Chiu (Ref 6) formula:

$$E_{exp} = E_s R \frac{KR + 2K - R}{2R - K + 1} \quad \text{(Eq 2)}$$

where $E_s$ is the Young's modulus of the substrate, $R = \frac{l_s}{l_c}$ is the relative thickness, and $K = -\frac{\varepsilon_s}{\varepsilon_c}$ is the relative strain. $l_s$ and $l_c$ are the thicknesses of the substrate and the coating.

The result obtained by this method is 124 GPa. (The difference between the value of the dynamic method and this one is about 10%.) The value is evaluated in a direction parallel to the coating beam. The equations and techniques presented in this paper provide a reasonable means of determining the elastic modulus of the coating layer.

## 4. Summarizing Remarks

Plasma-sprayed coatings present a new range of inspection and monitoring problems requiring further development. Whatever their intended use may be, the properties, structure, functional characteristics, and performance all depend, among other things, on adhesion between the coating and the substrate. The

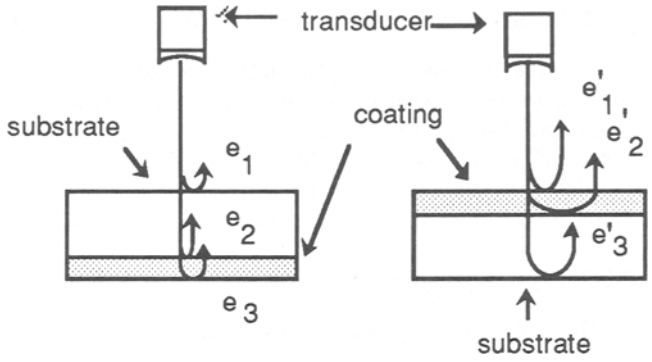


**Fig. 10** The pulse echo technique investigated. Echoes $e_1$, $e_2$, and $e_3$, and $e'_1$, $e'_2$, and $e'_3$ are detected (Ref 4).

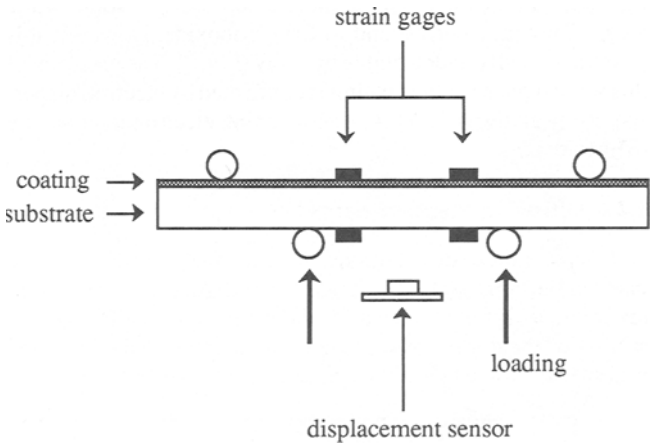


**Fig. 11** Location of the strain gages and loading

effect of microstructure should be considered because plasma-sprayed coatings have different levels of porosity and macrostructure than those of bulk materials.

## References


1. G.H. Liu, Mechanisms of Friction and Wear at High Temperature for Pure Ceramic Coatings or with Addition of Solid Lubricants (in French), Ph.D. thesis, ENSAM, ISMCM - Laboratoire de Tribologie, Paris, 1991
2. A. Tronche and P. Fauchais, Hard Coatings ($Cr_2O_3$ - WC-Co) Properties on Aluminium or Steel Substrates, *Mat. Sci. Eng.*, Vol 92, 1987, p 133-144
3. C.C. Chiu and E.D. Case, Elastic Modulus Determination of Coatings Layers as Applied to Layered Ceramic Composites, *Mat. Sci. Eng., A*, Vol 132, 1991, p 39-47
4. A. Vincent and A. Moughil, Ultrasonic Characterization of Zirconia Based Thermal Barriers, *NDT Int.*, Vol 22 (No. 5), 1989, p 283-291
5. H. Behnken and V. Hauk, *International Conference on Residual Stresses (ICRS2)*, G. Beck, S. Denis, and A. Simon, Ed., Elsevier Applied Science, 1988, p 314-346
6. C.C. Chiu, Determination of the Elastic Modulus and Residual Stresses in Ceramic Coatings using a Strain Gage, *J. Am. Ceram. Soc.*, Vol 73 (No. 7), 1990, p 1999-2005